Plasma Channel Diagnostic Based on Laser Centroid Oscillations

A. J. Gonsalves, K. Nakamura, C. Lin, J. Osterhoff, S. Shiraishi, C. B. Schroeder, C. G. R. Geddes, Cs. Tóth, E. Esarey, and W. P. Leemans

Lawrence Berkeley National Laboratory, Berkeley, CA 94720, USA

Abstract. A technique has been developed for measuring the properties of discharge-based plasma channels by monitoring the centroid location of a laser beam exiting the channel as a function of input alignment offset between the laser and the channel. The centroid position of low-intensity ($< 10^{14}\,\mathrm{Wcm}^{-2}$) laser pulses focused at the input of a hydrogen-filled capillary discharge waveguide was scanned and the exit positions recorded to determine the channel shape and depth with an accuracy of a few %. In addition, accurate alignment of the laser beam through the plasma channel can be provided by minimizing laser centroid motion at the channel exit as the channel depth is scanned either by scanning the plasma density or the discharge timing. The improvement in alignment accuracy provided by this technique will be crucial for minimizing electron beam pointing errors in laser plasma accelerators.

Keywords: discharges (electric), plasma accelerators, plasma density, plasma diagnostics
PACS: 52.70.Kz, 52.38.Kd, 52.80.-s, 52.25.-b

INTRODUCTION

Laser-driven plasma accelerators (LPAs) [1] have shown acceleration gradients orders of magnitude higher than those found in conventional accelerators, offering the potential for a significant reduction in accelerator length and cost. Recent progress, such as the production of high-quality GeV electron beams in just a few cm [2, 3] has increased interest in laser-plasma accelerator technology as a driver for radiation sources – ranging from coherent THz [4] to free electron laser (FEL) x-ray sources [5] and Thomson scattering gamma ray sources [6] – and as a path towards a TeV-class linear collider [7].

Pre-formed plasma channels can be used to mitigate diffraction of the laser pulse and increase the energy gain of an LPA. This has allowed for GeV energy gain using only 40 TW of laser power [2, 3] but also allows for operation in the quasi-linear regime for controlled acceleration in a dark-current free accelerator. In order to realize such an LPA, the transverse density profile of the plasma must be carefully controlled for efficient guiding and acceleration. Therefore accurate methods to measure the density profile are important.

Interferometry is commonly used for measuring plasma channel profiles. For the hydrogen-filled capillary discharge waveguide used in GeV acceleration experiments at LBNL, interferometric experiments required the capillary length to be less than a few mm in the case of longitudinal interferometry (resulting in measurement errors due to end effects), or square, transparent capillaries (and assumptions on symmetry) for transverse interferometry [8, 9]. Spot size measurements at the output of the capillary have also been used to deduce channel depth [10], but this technique does not provide the channel shape and is sensitive to the mode quality of the probe laser pulse.

In this paper, the centroid location of low-intensity ($< 10^{14}\,\mathrm{Wcm}^{-2}$) laser pulses at the output of a plasma channel is used to measure the properties of the channels, including alignment, depth, and profile. Whereas laser pulses of intensity $> 10^{18}\,\mathrm{Wcm}^{-2}$ are used for laser plasma acceleration, the intensity was kept low in these experiments so that non-linear effects such as self-focusing [11] could be neglected and the plasma properties measured in a straightforward way. The technique relies on the fact that a transverse offset of the laser pulse at the entrance of the plasma channel causes the laser beam to undergo transverse oscillations about the channel axis. These oscillations depend on the initial centroid offset and angle with respect to the channel axis, and on the channel properties. As will be shown, measuring the dependence of the exit laser centroid position on the input and on channel formation timing provides direct information on the channel matched spot size and profile. This technique reduces the measurement error compared to interferometry and provides increased precision in channel alignment to minimize pointing errors in LPA applications [12].

CP1299, *Advanced Accelerator Concepts: 14th Workshop*, edited by S. H. Gold and G. S. Nusinovich

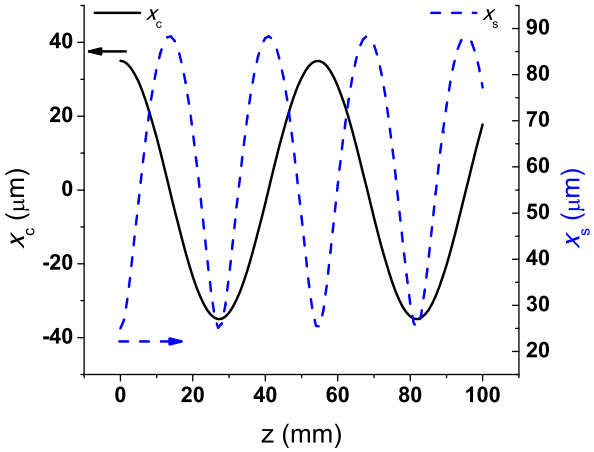

FIGURE 1. Laser centroid offset x_c (solid line) and spot size (dashed line) as a function of propagation distance z in a channel of matched spot size $r_m = 47\,\mu m$ for an input centroid offset of $x_{ci} = 35\,\mu m$, input injection angle $\theta_i = 0$, and initial spot size $r_i = 25\,\mu m$.

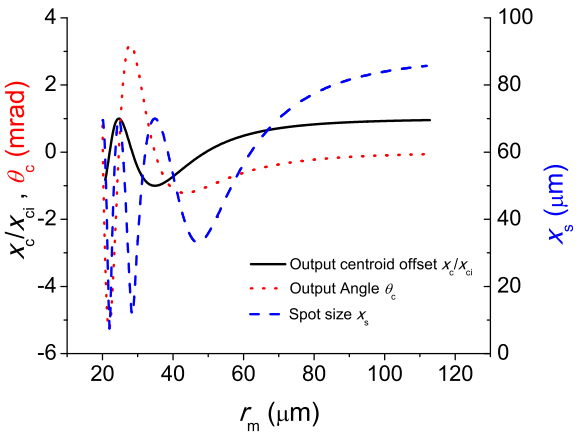

FIGURE 2. Laser beam parameters at the output of a plasma channel of length 15 mm as a function of matched spot size. Normalized laser centroid offset x_c/x_{ci} (solid line), angle (dotted line), and spot size (dashed line) are shown for an input centroid offset of $x_{ci} = 10\,\mu m$, input injection angle $\theta_i = 0$, and $r_i = 80\,\mu m$.

LASER PROPAGATION IN A PLASMA CHANNEL

To understand how the propagation of a laser beam through a longitudinally-uniform plasma channel is affected by pointing errors, this section discusses the basic physics for low-intensity laser pulses with power below the critical power for self-focusing, including an initial centroid offset x_{ci} and injection angle θ_i. It will be shown that the evolution of the centroid position depends only on the density profile and that measuring the dependence of the laser centroid movement at the exit of a plasma channel on the input offset can yield the matched spot size r_m [i.e., the spot size for which the laser beam propagates with constant spot size $r_s(z) = r_m$] .

Equations describing the behavior of the laser spot size $r_s(z)$ and centroid $x_c(z)$ have been derived by analyzing the paraxial wave equation for the envelope of the laser including the effects of a preformed parabolic density channel $n(x,y) = n_0 + \Delta n(x^2+y^2)/r_m^2$, where Δn is the channel depth at the radius of the matched spot r_m [13]. Consider a laser pulse with a Gaussian intensity profile such that $|a|^2 = (a_0 r_0/r_s)^2 \exp\left(-2r^2/r_s^2\right)$, where a_0 is the normalized laser vector potential given by $a_0^2 \simeq 7.3\times10^{-19}(\lambda\,[\mu m])^2 I_0[\mathrm{Wcm}^{-2}]$, λ is the laser wavelength, r_0 is the spot size of the vacuum focus, and r is the distance from the laser centroid $r^2 = (x-x_c)^2 + (y-y_c)^2$ with x_c and y_c the centroid locations in the x and y directions. For laser pulses where the head-to-tail centroid displacements are much smaller than the spot size (valid for laser pulse length $L_p \ll Z_m$), and $x_c \lesssim r_s$, $a^2 \ll 1$, and $k_p^2 r_0^2 \gg 1$, the centroid location is

$$x_c = x_i \cos\left[(k_{\beta c} z) - \varphi\right], \tag{1}$$

where the initial phase $\varphi = \arccos(x_{ci}/x_i)$ and oscillation amplitude $x_i = [x_{ci}^2 + \theta_i^2 k_{\beta c}^{-2}]^{1/2}$ depend on the initial injection centroid offset x_{ci} and injection angle θ_i, and $k_{\beta c} = Z_m^{-1}$ is the wavenumber of the laser centroid oscillation about the plasma channel axis assuming $\Delta n = \Delta n_c$. The period of the centroid oscillation does not depend on the laser power but only on the matched spot size of the channel r_m.

For $r_s = r_i$ and $dr_s/dz = 0$ at the channel entrance ($z = 0$), the spot size evolution is

$$r_s^2 = 0.5 r_i^2\left[1 + r_m^4/r_i^4 + \left(1 - r_m^4/r_i^4\right)\cos(2k_{\beta c} z)\right]. \tag{2}$$

The spot size therefore oscillates between r_i (the value at the channel entrance) and r_m^2/r_i at twice the frequency of the centroid oscillation. This is shown in Fig. 1, where the laser centroid (solid line) and the spot size (dashed line) are shown as a function of propagation distance z in a channel of matched spot size $r_m = 47\,\mu m$ for an input centroid offset of $x_{ci} = 35\,\mu m$ and initial spot size $r_i = 25\,\mu m$.

Figure 2 shows the laser offset normalized by input offset x_c/x_{ci} (solid line), the laser angle (dotted line), and the spot size (dashed line) at the output of a plasma channel of length 15 mm as a function of r_m as calculated from Eqs. (1) and (2) for $\theta_i = 0$, $x_{ci} = 10\,\mu$m, and $r_i = 80\,\mu$m. For a given centroid offset or laser spot size at the output of the waveguide, more than one solution to the matched spot size may exist.

Determination of the matched spot size r_m using the laser centroid, spot size, or angle can be accomplished by several methods. For capillary discharge waveguides an experimentally straightforward method is to rely on the property that the plasma channel depth continuously decreases on the nanosecond timescale (and the matched spot size increases) after the peak of the discharge as shown in [14, 15]. The delay between the onset of the plasma channel and arrival of the laser pulse scans the matched spot size from infinity at long delays where there is no discharge current to finite sizes (i.e., scanning right to left in Fig. 2). By measuring the laser spot size this technique has been applied to determine the matched spot size of a hydrogen-filled capillary discharge waveguide [10]. However, these measurements can be difficult to interpret if the laser mode is not Gaussian [12]. For all higher-order modes the spot size and centroid evolution are described by Eqs. (1) and (2) in the low-power limit, and to recover the channel properties requires precise knowledge of the input and output modes. Understanding the mode propagation may require modal decomposition or wavefront analysis.

The matched spot size of a parabolic channel can be obtained by measuring the centroid location at the channel exit as a function of initial offset. The solution to Eq. (1) is

$$r_m = \sqrt{2z/\left(k\left|\cos^{-1}\left(dx_c/dx_{ci}\right) + 2\pi j\right|\right)} \tag{3}$$

The integer j can be determined by measuring the response of the laser to discharge timing. It should be noted from Eq. (3) that only the gradient dx_c/dx_{ci} is used in the calculation of r_m and knowledge of the location of the channel axis is not required. Furthermore, the gradient is independent of the input laser angle θ_i, which adds a constant offset to x_c. Since using the slope measurement does not depend on the precise alignment of the capillary, it offers increased accuracy for determining the matched spot size compared with measuring the timing dependence alone.

The centroid oscillation can be used to retrieve not only the channel matched spot size but also its profile. Measurement of channel profile by measuring laser output centroid versus input is illustrated in Fig. 3. The laser centroid shift was calculated for channels with density profiles $n(r) = n_0 + \Delta n r^2/r_m^2$ and $n(r) = n_0 + \Delta n r^4/r_m^4$ and length 15 mm for a matched spot of 47 μm (the density rise at $r = 47\,\mu$m is held constant). These curves were generated

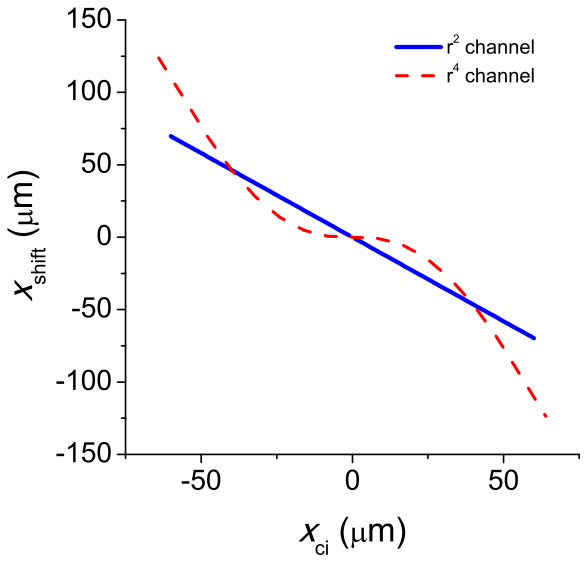

FIGURE 3. Calculated laser centroid shift $x_{shift} = x_c - x_{ci}$ at the output of a plasma channel of length 15 mm as a function of input laser centroid offset for channels of shape r^2 and r^4 for $r_m = 47\,\mu$m.

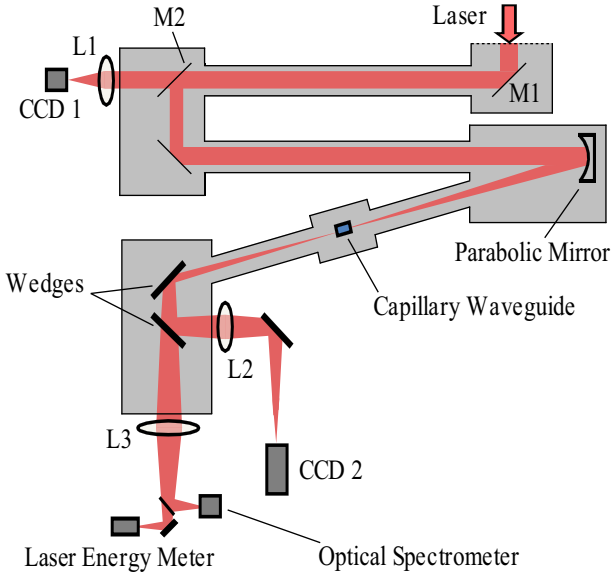

FIGURE 4. The experimental layout used for investigating laser propagation in a hydrogen-filled capillary discharge waveguide.

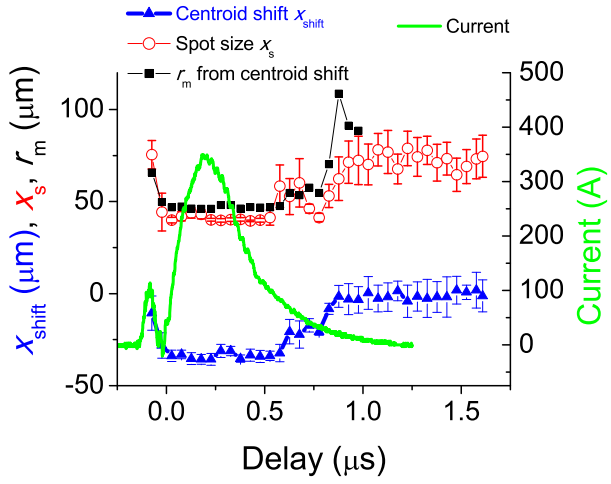

FIGURE 5. Measured centroid shift (blue triangles) and spot size r_s in the x direction (x_s, red circles) as a function of delay between arrival of the laser pulse and onset of the discharge. The green line shows the discharge current. The matched spot size as calculated from the laser centroid shift using Eq. (3) is shown by the black squares.

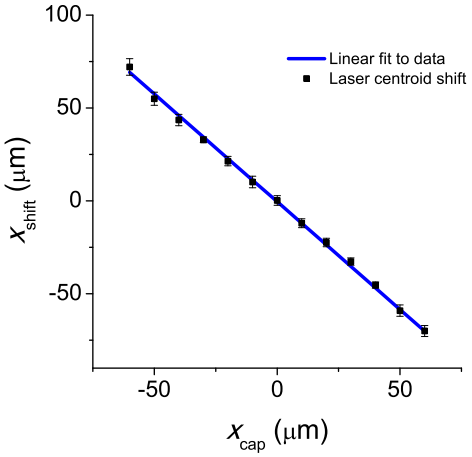

FIGURE 6. Measured centroid shift (squares), as a function of input laser centroid offset for a capillary of diameter 300 μm and length 15 mm and delay 225 ns. The linear fit (solid line) is equivalent to fitting a parabolic shape to the channel.

using ZEMAX by calculating the path of rays offset from the axis. For the case of a parabolic channel, the curve is linear as is expected from Eq. (1), since z (the capillary length) is constant. For the case of a channel with r^4 dependence, rays away from the axis experience a stronger deflection and the curve in Fig. 3 becomes non-linear. By using ray-tracing and adjusting the fitted channel shape to match measured data, the channel shape can be retrieved.

In the subsequent section, experiments will be described in which the evolution of the plasma channel in a hydrogen-filled capillary discharge waveguide is deduced from measurements of the laser centroid shift.

EXPERIMENTAL SETUP AND RESULTS

The experimental layout is shown in Fig. 4. Low energy pulses (<5 mJ) from a Ti:sapphire laser system were focused onto the entrance of a hydrogen-filled capillary discharge waveguide by a 2 m focal length off-axis parabolic mirror [2, 3]. The hydrogen-filled capillary discharge waveguide has been described in detail elsewhere [8, 16, 9], along with its use for laser wakefield acceleration of electrons to energies up to 1 GeV [2, 3].

An aperture 2 cm in diameter was used to increase the effective f-number of the focusing system compared to previous experiments [2, 3], resulting in beams with a spot size of $r_i = 70\,\mu$m at the capillary entrance. The large focal spot allowed for the unguided beam to pass through the 15 mm-long and 300 μm-diameter capillary with minimal wall interaction since the Raleigh range is $Z_R = 19$ mm. Thus the centroid location at the output of the capillary when there is no plasma channel ($r_m = \infty$) (i.e., when no current flows through the capillary) was the same as when the capillary was removed. The laser energy on target was 0.5 mJ, corresponding to a peak intensity of 5×10^{13} Wcm^{-2} for a pulse length of 120 fs. Since this pulse length of 36 μm is much shorter than the typical centroid oscillation wavelength of ~ 10 mm, head-to-tail displacements can be neglected and spot size and centroid motions are decoupled. The low laser energy and pulse length longer than for optimized compression ensured that the intensity was below the ionization threshold of hydrogen ($\sim 10^{14}$ Wcm^{-2}), avoiding ionization-induced diffraction [17], and that the power was below the self-focusing limit (i.e., $P \ll P_c$), allowing the evolution of the laser spot size to be described by Eq. (2).

Hydrogen gas filled the capillary to a pressure of 46 Torr via slots located 0.5 mm from each end. The on-axis density for delays after which a stable plasma channel is formed was calculated to be 1.4×10^{18} cm^{-3} using the scaling given in Ref. [9].

Laser radiation emerging from the capillary was attenuated by reflection off two optically flat glass wedges. The pulses were refocused by a lens of focal length 500 mm, allowing for imaging of the output of the capillary onto a 12-bit CCD camera that measures the centroid location and spot size of the laser beam.

The laser centroid shift due to the plasma channel $x_{\rm shift} = x_{\rm c} - x_{\rm ci}$ at the capillary output was determined after thresholding the image to 50% of the peak, and is plotted versus delay in Fig. 5 along with the discharge current for an input offset of $x_{\rm ci} = 30\,\mu$m. For delays during the discharge, the laser centroid is shifted and the spot size reduced, consistent with the existence of a plasma channel. The centroid shift increases during the first 200 ns to an approximately constant value for approximately 600 ns. For delays after this, when the discharge current drops below 100 A, the shift begins to return to zero and the spot size increases to the value observed without the capillary in place. This is expected since after the current has decayed there is no plasma channel and the matched spot goes to infinity.

The matched spot was obtained by scanning backwards in delay (see Fig. 5), which is effectively equivalent to scanning from infinite to finite $r_{\rm m}$ in Fig. 2. The matched spot can then be uniquely determined with the assumption $\theta_{\rm i} = 0$ using Eq. (3) with $dx_{\rm c}/dx_{\rm ci} = x_{\rm c}/x_{\rm ci}$ and $j = 0$. The calculated values for $r_{\rm m}$ are shown by the black squares in Fig. 5. For delays where the current remains above 100 A, the average matched spot calculated from the centroid shift is $46.9 \pm 0.8\,\mu$m, which is in excellent agreement with $46.5\,\mu$m given by the scaling derived from simulations [18]. It should be noted that the accuracy of measurement of the matched spot size is less than 2% compared with 20% in previous interferometry measurements [9].

Measurement of the laser centroid as a function of discharge delay also provides an accurate method of aligning the capillary and laser beam. For a properly aligned channel there will be no dependence of the centroid shift on the delay time between laser pulse arrival and initiation of the discharge. The alignment error is dominated by the accuracy of centroid determination, which for these experiments was approximately $5\,\mu$m, limited by the level of magnification of the imaging system for the capillary output. This is significantly better than other techniques that rely on optimizing throughput or modal shape and typically allow for alignment precision to within $\sim 20\,\mu$m. With a higher magnification of the imaging system, it is expected that the alignment accuracy of the centroid motion based technique could be lowered to $\sim 1\,\mu$m. This improvement in accuracy of capillary alignment is expected to prove crucial for LPAs since a μm change in alignment can potentially lead to a mrad change in electron beam pointing.

Measurement of the channel shape was achieved by recording the output laser centroid location versus input location at fixed delay. Figure 6 shows the output-input data, taken at a constant delay of $t_{\rm delay} = 225$ ns for the same parameters as Fig. 5. The linear dependence implies a parabolic plasma channel over the extent of the matched spot. Close to the wall the density has been shown to rise faster than r^2 since the temperature gradient increases [9, 14, 18], which is difficult to probe using this technique since large offset would cause clipping of the beam at the capillary entrance and wall guiding can change the oscillation period. However this effect is not important since for matched guiding there is negligible laser energy close to the wall.

The gradient of the line in Fig. 6 also provides a measurement of the matched spot of a parabolic channel and is more accurate than calculation based on a single value of $x_{\rm cap}$ (as was done for Fig. 5) since it is independent of the input angle $\theta_{\rm i}$ and centroid offset $x_{\rm ci}$. A linear fit to the data gives $r_{\rm m} = 47\,\mu$m using Eq. (3), where $j = 0$ was determined from the fact that the centroid shift undergoes less than half an oscillation in Fig. 5. This is consistent with $r_{\rm m} = 46.5\,\mu$m given by the scaling derived from simulations [18].

DISCUSSION

The motion of low-power ($P \ll P_{\rm c}$) laser pulses in a plasma channel for the case of finite offset between the laser and plasma channel axes has been investigated. It was shown that the laser centroid offset at the capillary output due to off-axis injection of the laser pulse could be used to determine the plasma channel depth and shape. Even though the method cannot provide information on the axial electron density, the low-power matched spot can be determined to a high degree of accuracy. The improved accuracy in measuring $r_{\rm m}$ is important for optimizing guiding in laser wakefield experiments. Measurements of the matched spot size and density profile in a hydrogen-filled capillary discharge waveguide using this technique were in excellent agreement with previously published scaling laws [18] and showed that the channel shape was parabolic within the radius of the matched spot. It was also found that the laser centroid measurements provide a way to align the plasma channel with improved accuracy.

Laser centroid motion can result in electron beam centroid motion in an LPA. If the betatron wavelength of an injected electron beam is less than the laser centroid oscillation wavelength, which is the case for typical LPA parameters, then the electron beam will track the laser pulse and likewise undergo oscillations in the channel, exiting the plasma in the laser direction. Laser pointing jitter is therefore a mechanism for increasing electron beam pointing jitter in a channel-guided laser plasma accelerator and it might be expected that use of a waveguide would increase electron beam jitter. However, the lowest reported value for the electron beam pointing jitter of 0.7 mrad rms was achieved through the use of a capillary waveguide [19]. Pointing jitter of 1.4 mrad rms has been achieved in a gas cell

[20], which is several times lower than that typically observed in unguided experiments [21]. Other effects such as the stability and homogeneity of the plasma and laser profiles will need to be investigated to understand the differences in electron beam pointing jitter between the guided and unguided LPA experiments.

To minimize laser and electron beam pointing errors in laser plasma accelerators, several strategies can be followed. Laser beam pointing control will need to be improved to well below the μrad level to ensure that x_i is minimized. For the parameters presented here, μrad jitter in laser pointing (typical of current laser systems) at the plasma channel input can cause mrad deviations in the laser angle during propagation through the plasma channel for $x_{ci} \approx 10\,\mu m$. Since the electron beam will follow the laser beam trajectory (provided the electron beam betatron oscillation wavelength is much smaller than the laser centroid oscillation wavelength), the plasma channel length should be tailored to allow for an integer number of betatron oscillations. This ensures that even in the presence of spatial offsets of the laser beam centroid, angular deflections at the exit of the plasma channel will be near or at zero value.

ACKNOWLEDGMENTS

The authors would like to thank N. Matlis, G. Plateau, J. van Tilborg, and E. Cormier-Michel for useful discussions. We appreciate contributions from D. Panasenko, D. Syversrud, and N. Ybarrolaza. This work was supported by the Director, Office of Science, Office of High Energy Physics, of the U.S. Department of Energy under Contract No. DE-AC02-05CH11231, and the Defense Advanced Research Projects Agency (DARPA).

REFERENCES

1. E. Esarey, C. B. Schroeder, and W. P. Leemans, *Rev. Mod. Phys.* **81**, 1229–1285 (2009).
2. W. P. Leemans, B. Nagler, A. J. Gonsalves, C. Tóth, K. Nakamura, C. G. R. Geddes, E. Esarey, C. B. Schroeder, and S. M. Hooker, *Nat. Phys.* **2**, 696–699 (2006).
3. K. Nakamura, B. Nagler, C. Tóth, C. G. R. Geddes, C. B. Schroeder, E. Esarey, W. P. Leemans, A. J. Gonsalves, and S. M. Hooker, *Phys. Plasmas* **14**, 056708 (2007).
4. W. P. Leemans, C. G. R. Geddes, J. Faure, C. Tóth, J. van Tilborg, C. B. Schroeder, E. Esarey, G. Fubiani, D. Auerbach, B. Marcelis, M. A. Carnahan, R. A. Kaindl, J. Byrd, and M. C. Martin, *Phys. Rev. Lett.* **91**, 074802 (2003).
5. F. Grüner, S. Becker, U. Schramm, M. Fuchs, R. Weingartner, D. Habs, J. Meyer-ter Vehn, M. Geissler, M. Ferrario, L. Serafini, B. van der Geer, H. Backe, W. Lauth, and S. Reiche, *Appl. Phys. B* **86**, 431 (2007).
6. P. Tomassini, A. Bacci, J. Cary, M. Ferrario, A. Giulietti, D. Giulietti, L. A. Gizzi, L. Labate, L. Serafini, V. Petrillo, and C. Vaccarezza, *IEEE Trans. Plasma Sci.* **36**, 1782 (2008).
7. W. P. Leemans, and E. Esarey, *Phys. Today* **62**, 44–49 (2009).
8. D. J. Spence, and S. M. Hooker, *J. Opt. Soc. Am. B* **17**, 1565–1570 (2000).
9. A. J. Gonsalves, T. P. Rowlands-Rees, B. H. P. Broks, J. J. A. M. van der Mullen, and S. M. Hooker, *Phys. Rev. Lett.* **98**, 025002 (2007).
10. P. S. Antsiferov, M. R. Akdim, and H. T. van Dam, *Rev. Sci. Instrum.* **78**, 123107–3 (2007).
11. E. Esarey, P. Sprangle, J. Krall, and A. Ting, *IEEE J. Quantum Electron.* **33**, 1879–1914 (1997).
12. A. J. Gonsalves, K. Nakamura, C. Lin, J. Osterhoff, S. Shiraishi, C. B. Schroeder, C. G. R. Geddes, C. Toth, E. Esarey, and W. P. Leemans, *Phys. Plasmas* **17**, 056706 (2010).
13. P. Sprangle, J. Krall, and E. Esarey, *Phys. Rev. Lett.* **73**, 3544–3547 (1994).
14. B. H. P. Broks, K. Garloff, and J. J. A. M. van der Mullen, *Phys. Rev. E* **71**, 016401 (2005).
15. B. H. P. Broks, W. Van Dijk, J. J. A. M. van der Mullen, A. J. Gonsalves, T. P. Rowlands-Rees, and S. M. Hooker, *Phys. Plasmas* **14**, 023501 (2007).
16. A. Butler, D. J. Spence, and S. M. Hooker, *Phys. Rev. Lett.* **89**, 185003 (2002).
17. W. P. Leemans, C. E. Clayton, W. B. Mori, K. A. Marsh, P. K. Kaw, A. Dyson, C. Joshi, and J. M. Wallace, *Phys Rev A* **46**, 1091 (1992).
18. B. H. P. Broks, W. van Dijk, and J. J. A. M. van der Mullen, *J. Phys. D Appl. Phys.* **39**, 2377 (2006).
19. A. J. Gonsalves, E. Esarey, C. G. R. Geddes, W. P. Leemans, C. Lin, K. Nakamura, D. Panasenko, C. B. Schroeder, and C. Tóth, "Longitudinal Density Tailoring For The Enhancement Of Electron Beams In The Capillary-Discharge Laser-Guided Wakefield Accelerator," in *PAC09*, JACOW, Vancouver, 2009.
20. J. Osterhoff, A. Popp, Z. Major, B. Marx, T. P. Rowlands-Rees, M. Fuchs, M. Geissler, R. Hörlein, B. Hidding, S. Becker, E. A. Peralta, U. Schramm, F. Grüner, D. Habs, F. Krausz, S. M. Hooker, and S. Karsch, *Phys. Rev. Lett.* **101**, 085002 (2008).
21. S. P. D. Mangles, A. G. R. Thomas, O. Lundh, F. Lindau, M. C. Kaluza, A. Persson, C. G. Wahlstrom, K. Krushelnick, and Z. Najmudin, *Phys. Plasmas* **14**, 056702 (2007).